Electronic Supplementary Material (ESI) for Journal of Materials Chemistry A.

Supplementary Information

Regulation of surface oxygen activity in Li-rich layered cathodes using band-alignment of vanadium phosphate surface coatings

Tristram Jenkins[1,2], Jose A. Alarco[1,2,3], Bruce Cowie[4], Ian D.R. Mackinnon[1,2]*

[1]Faculty of Science, [2]Centre for Clean Energy Technologies and Practices,
[3]Centre for Materials Science, Queensland University of Technology, Brisbane 4001 Australia.
[4] Australian Synchrotron, 800 Blackburn Road, Clayton, Victoria 3168 Australia.

Keywords: Li-Ion Batteries, Phosphates, X-ray Absorption Spectroscopy, Electronic Structure, $Li_3V_2(PO_4)_3$, Cathode Materials, $Na_3V_2(PO_4)_3$, Vanadium Phosphate, Li-rich layered oxide, Li-rich manganese layered oxide

*Corresponding Author: Tristram Jenkins
Tristram.jenkins@hdr.qut.edu.au

Carbonate Precursor Synthesis

Pristine Li-rich layered oxide $Li_{1\cdot2}Ni_{0\cdot13}Co_{0\cdot13}Mn_{0\cdot54}O_2$ (LLO) was prepared by solid-state reaction of lithium hydroxide monohydrate ($LiOH\cdot H_2O$) and the transition metal carbonate precursor, $Mn_{0.675}Co_{0.1625}Ni_{0.1625}CO_3$. The transition metal carbonate precursor was obtained via controlled co-precipitation using a continuously stirred reaction vessel. A 2M aqueous transition metal solution was prepared using $MnSO_4\cdot H_2O$, $NiSO_4\cdot 6H_2O$, and $CoSO_4\cdot 7H_2O$ (99.99%, Sigma Aldrich) at molar ratio of 0.675:0.1625:0.1625. Then a single aqueous solution of 2M Na_2CO_3 with a concentration of 0.2M of $NH_4.H_2O$ was prepared as a dual buffer and complexation agent. The reaction vessel started with an initial volume of 0.2M ammonia hydroxide aqueous solution and kept at a temperature of 55 °C with stirrer speed of 800rpm for the 12hr total reaction time. The transition metal solution was dosed continuously for the first 4 hours of the reaction and the buffer/complexation agent was dosed actively to maintain a pH of 7.5–8.0 for the full duration of the reaction. The precipitate was filtered and washed at room temperature with a Na_2CO_3 solution and deionized water before vacuum-drying at 100 °C overnight to produce the transition metal carbonate precursor.

UPS and UV-VIS-NIR energy approximation:

For UPS, the Secondary Electron Cut-off ($E_{cut\text{-}off}$) was determined using the vertical intersection of linear slope at half maximal intensity. The E_{VBM} was determined at the linear intersection of the final low energy slope with zero intensity (y-axis). Ionization potential (IP) and Work function (WF) values were then calculated using the following formulas:

$$WF = h\nu - E_{cut-off} \quad \text{(hv=21.2eV for He I)}$$

$$IP = WF - E_{VBM}$$

The band gap energies of VP-LLO and LLO samples were determined using a Tauc plot conversion of UV-VIS-NIR reflectance spectra and a direct energy transition was assumed (n=2). A vertical intersection between the X-axis and a linear trend for the highest energy sloping region was taken as the fundamental energy gap with any subsequent gaps being treated secondary optical band gap transitions caused by defect states at grain boundaries or surface regions of the samples.

Electronic structure determination details:

To evaluate the effects of vanadium phosphate surface coatings on the electronic structure of pristine LLO material both DFT-based theoretical calculations and experimental techniques were used on the uncycled cathode materials. UV-VIS-NIR and UPS He I spectroscopy measurements were used to determine the intrinsic valance band maximum (E_{VBM}), work function (WF), Ionization Potential (IP) and bandgap energy (E_g) of pristine PR-LLO, LVP-LLO and NVP-LLO samples relative to their vacuum level [1]. For the UPS He I emission spectra, $E_{cut\text{-}off}$ was measured as 16.57 eV, 18.12 eV and 18.22 eV and E_{VBM} was measured at 2.75 eV, 3.12 eV and 3.79 eV for PR-LLO, LVP-LLO and NVP-LLO, respectively. WF and IP energy values were calculated for each sample relative to the vacuum level (see supplementary information for more detail). UV-VIS-NIR reflectance spectra for all samples and Tauc plots were constructed to determine the optical bandgap transition for pristine and VP-coated materials (Figure 3d).

Based on Tauc plot evaluation, the band gaps for PR-LLO, LVP-LLO and NVP-LLO were measured at 1.68 eV, 0.94 eV and 0.51 eV, respectively. The lower band gaps for VP-coated samples implies that there is overlap between the VP coating and the bulk LLO material. This overlap suggests facile electron conductivity for VP-coated particles compared with uncoated LLO. In addition, Urbach tail regions are present following secondary energy transitions, suggesting a degree of disorder or amorphous character at both the coated and uncoated sample surfaces [2] [3].

EIS method details:

Impedance spectra were analysed using a physical model which represents the combination of resistive/capacitive elements that likely exist in these samples. The constant phase elements and equivalent circuit are represented in Figure 6c. Table S2 shows the values that were extrapolated from the fitting procedure of the electrolyte resistance, R_e, surface resistance, R_s, and charge transfer resistance, R_{ct}. The Warburg impedance, W, is also provided in Table S2. In the high frequency region, the semicircle is comprised of two regions representing the initial lithium-ion diffusion across the solid/liquid interface (high frequency region) and the charge transfer region between the surface film and particle interface. The diameter of this region represents the charge transfer resistance (R_{ct}). This diameter is substantially reduced in VP-coated LVP-LLO and NVP-LLO, which present a lowered charge transfer resistance compared to PR-LLO. The linear region following this is the Warburg region, representing the bulk solid-state diffusion of Li-ions into the LLO material.

Supporting Figures:

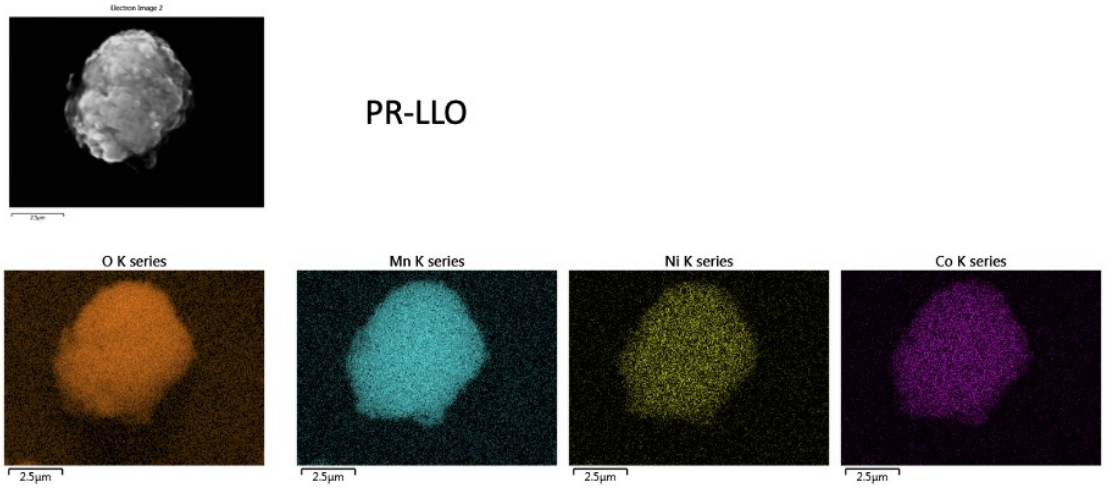

	O	Mn	Ni	Co
Wt%	63	24.8	6.7	5.6

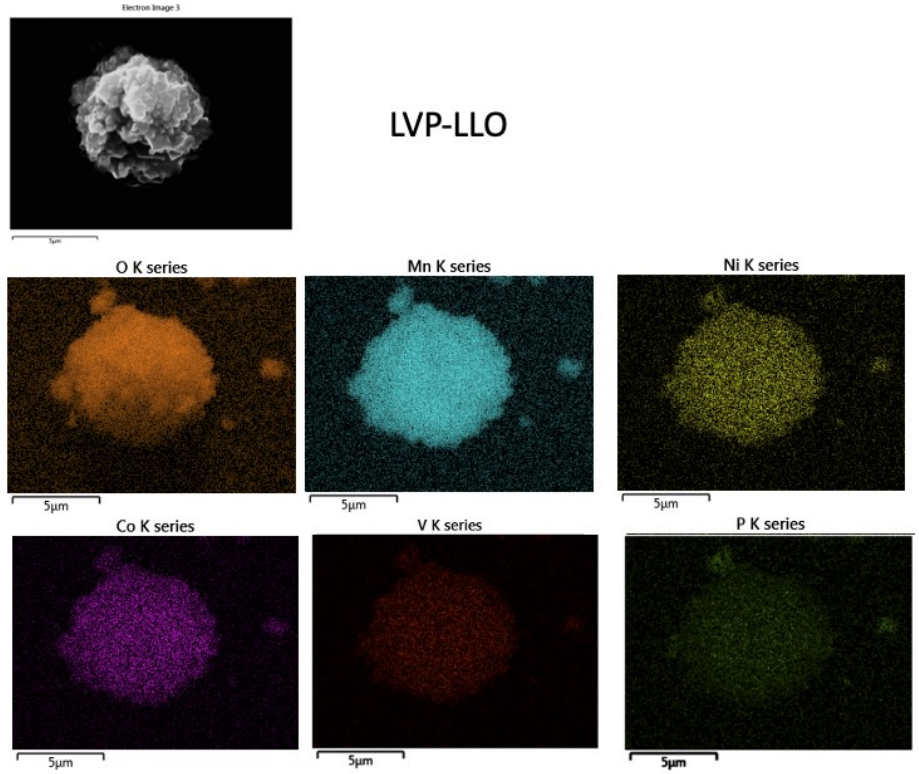

Symbol	Mn	O	Ni	Co	C	V	P
Wt%	37.11	32.86	9.74	8.33	8.16	2.21	1.59

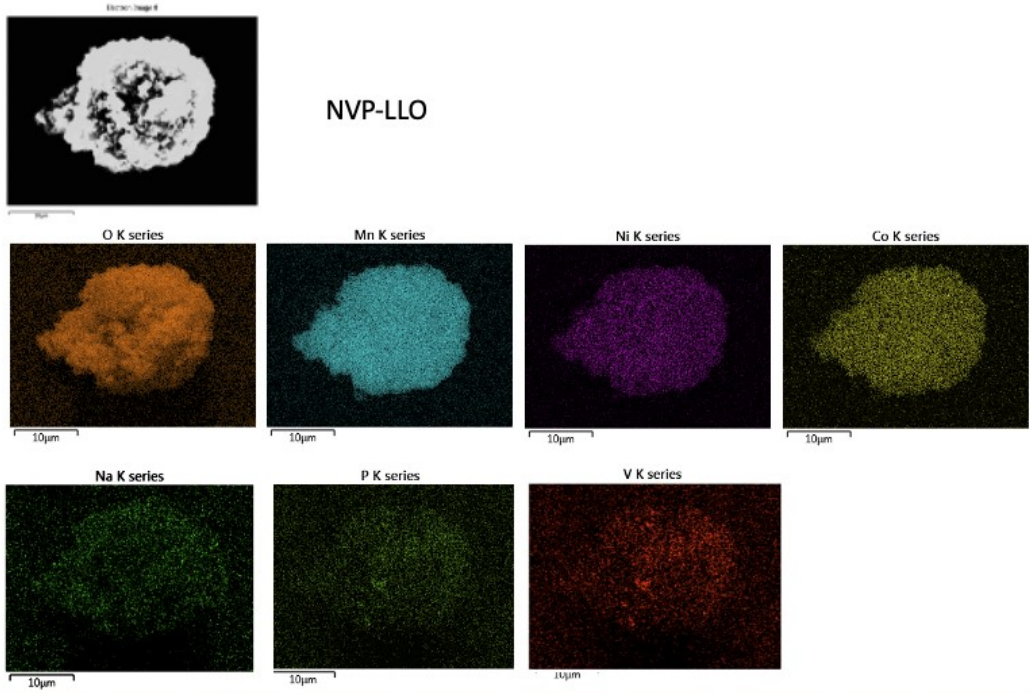

Element	Symbol	Mn	O	Ni	Co	C	V	P	Na
Weight	Conc.	38.89	34.3	9.97	7.98	5.85	1.23	0.96	0.81

Figure S1a-c. SEM-EDX elemental maps for PR-LLO (a), LVP-LLO (b) and NVP-LLO (c)

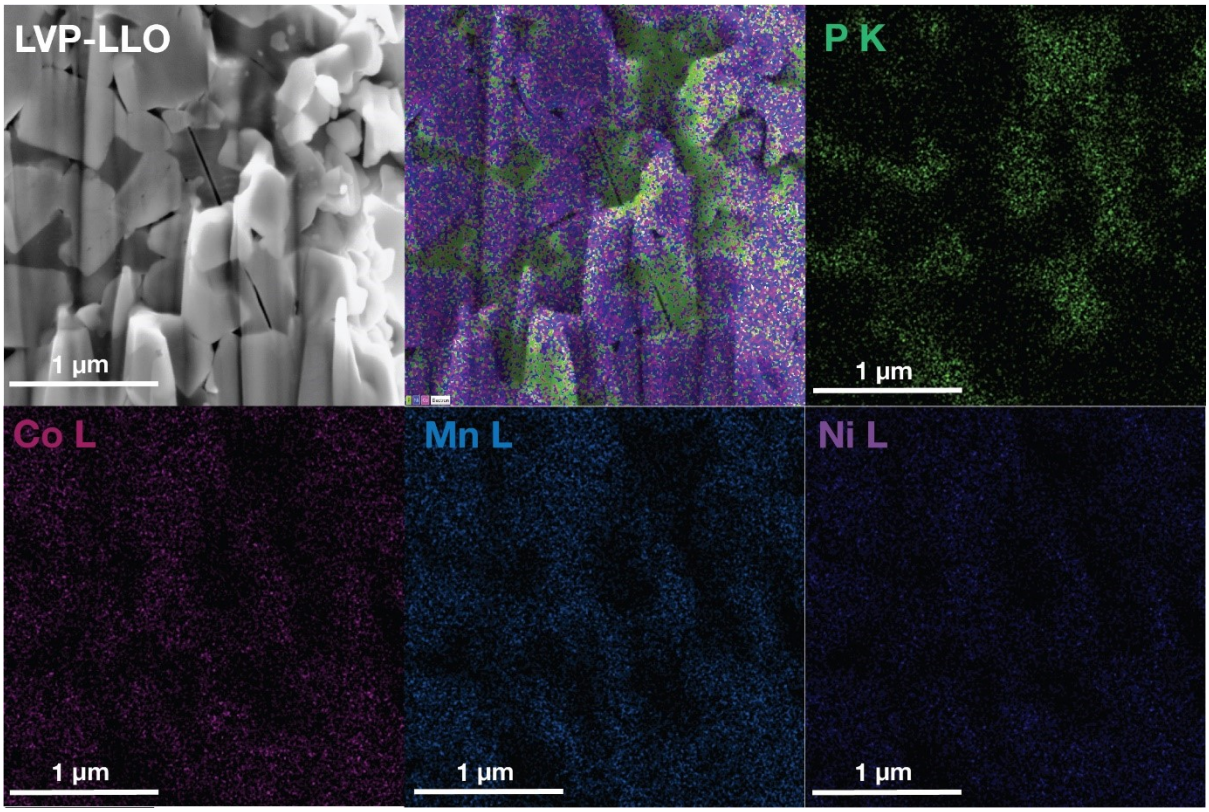
LVP-LLO
1 µm
P K
1 µm
Co L
1 µm
Mn L
1 µm
Ni L
1 µm

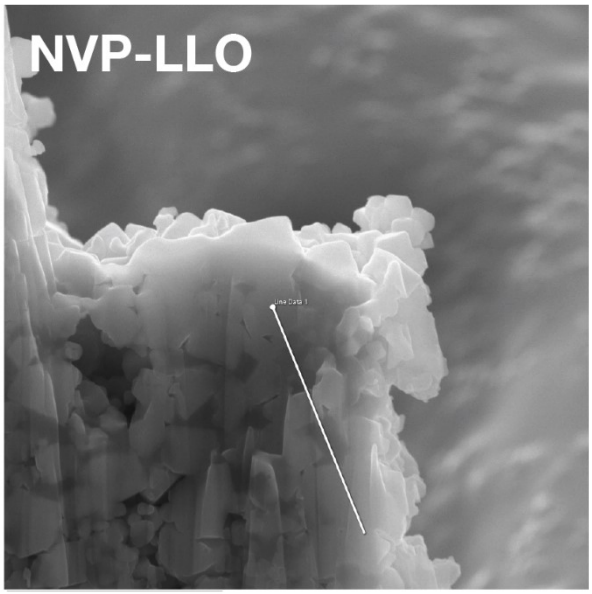

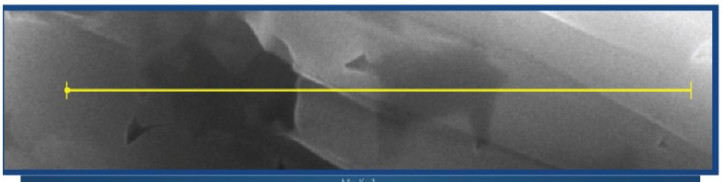

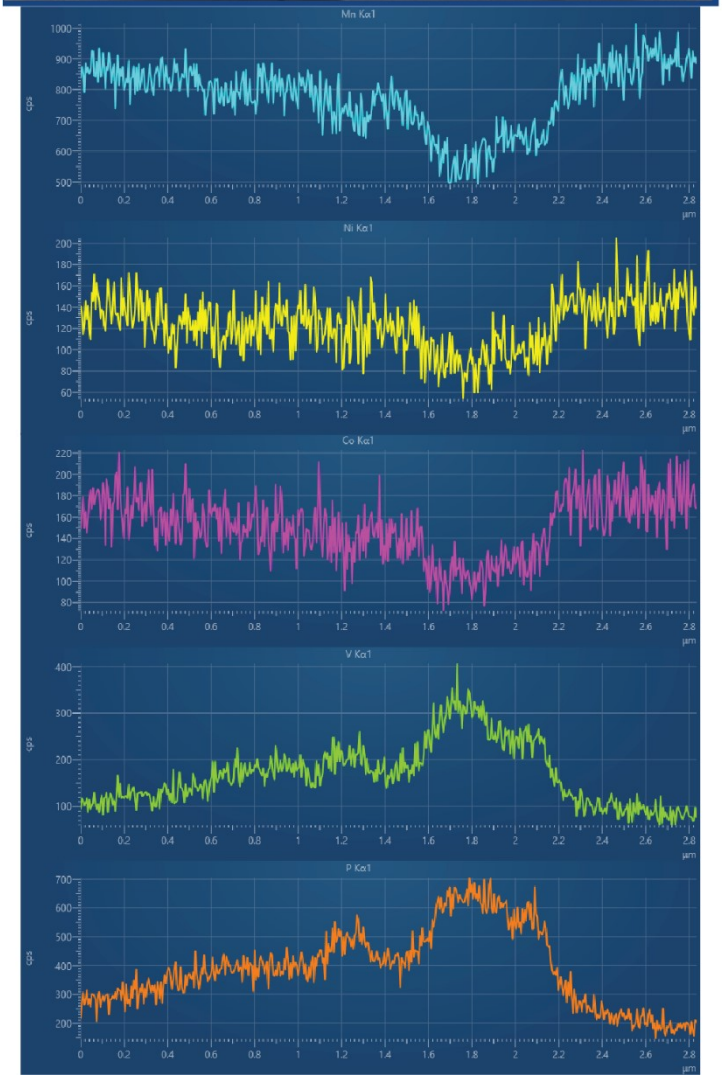

Mn

Ni

Co

V

P

Figure S2. FIB-SEM EDS data for a) LVP-LLO as cross section elemental map and b) NVP-LLO as cross-section elemental line scan (NOTE: for LVP-LLO EDS was collected at 5kV, due to low kV V L could not be resolved from O K and so both were excluded from the mapping).

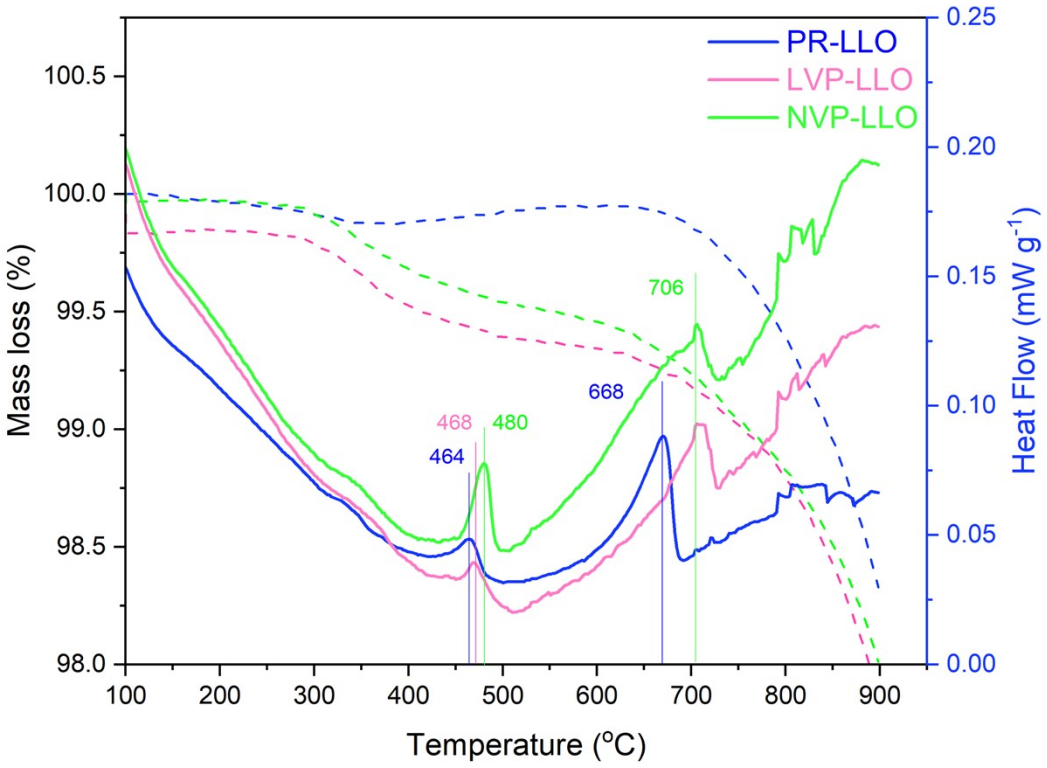

Figure S3. Thermogravimetric analysis and Differential Scanning Calorimetry measurements from 25°C – 900°C under N_2 of a) PR-LLO (blue) b) LVP-LLO (purple) and c) NVP-LLO (green) Pristine powder samples (NOTE: mass loss at ~350°C across all VP-coated LLO samples is attributed to carbonization of leftover organic contaminants (i.e. Carbon, nitrogen) from the VP coating procedure due to trace Air in the N_2 gas line.)

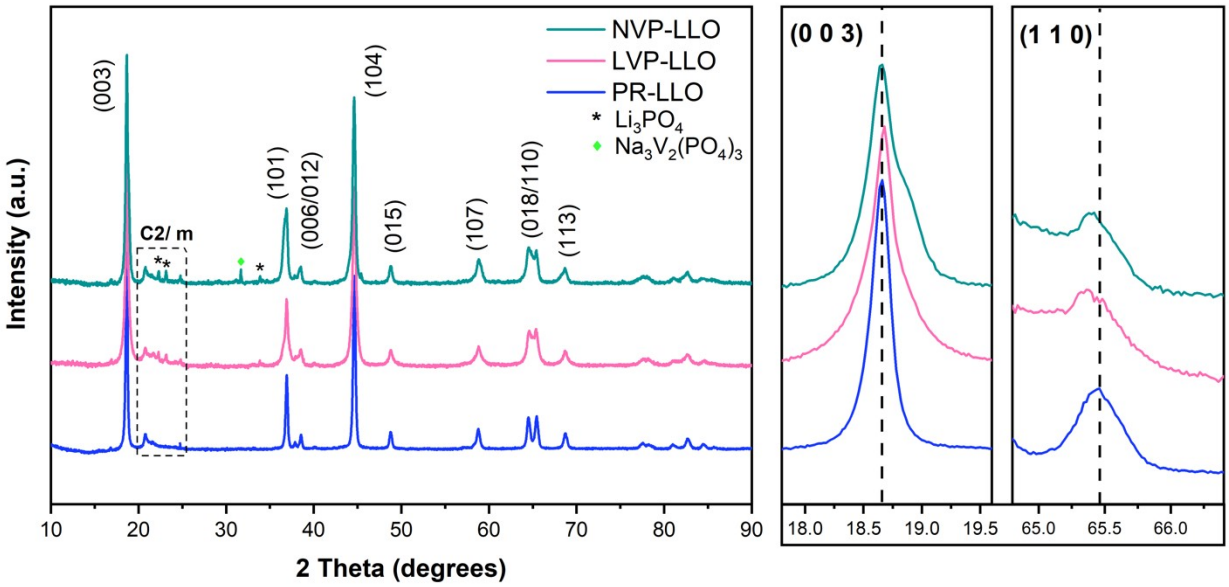

Figure S4. XRD diffraction patterns for PR-LLO, LVP-LLO and NVP-LLO samples with magnified view of the (0 0 3) and (1 1 0) peak regions assigned to the $R\bar{3}M$ $LiTMO_2$ phase.

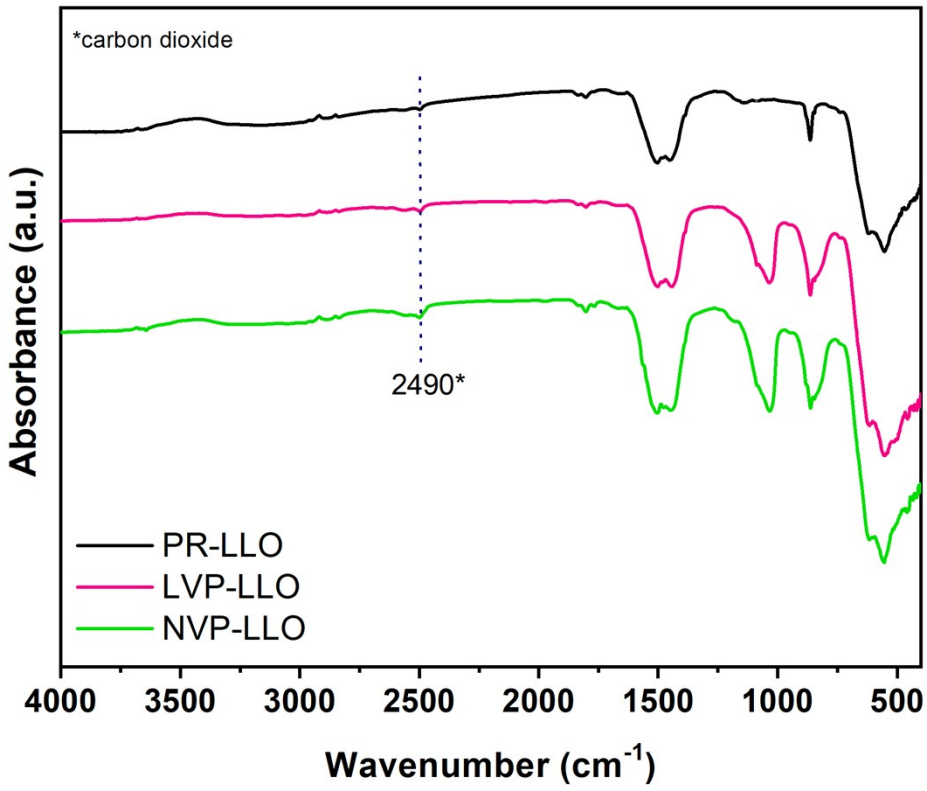

Figure S5. FTIR spectra for PR-LLO, LVP-LLO and NVP-LLO samples (4000-400 cm^{-1})

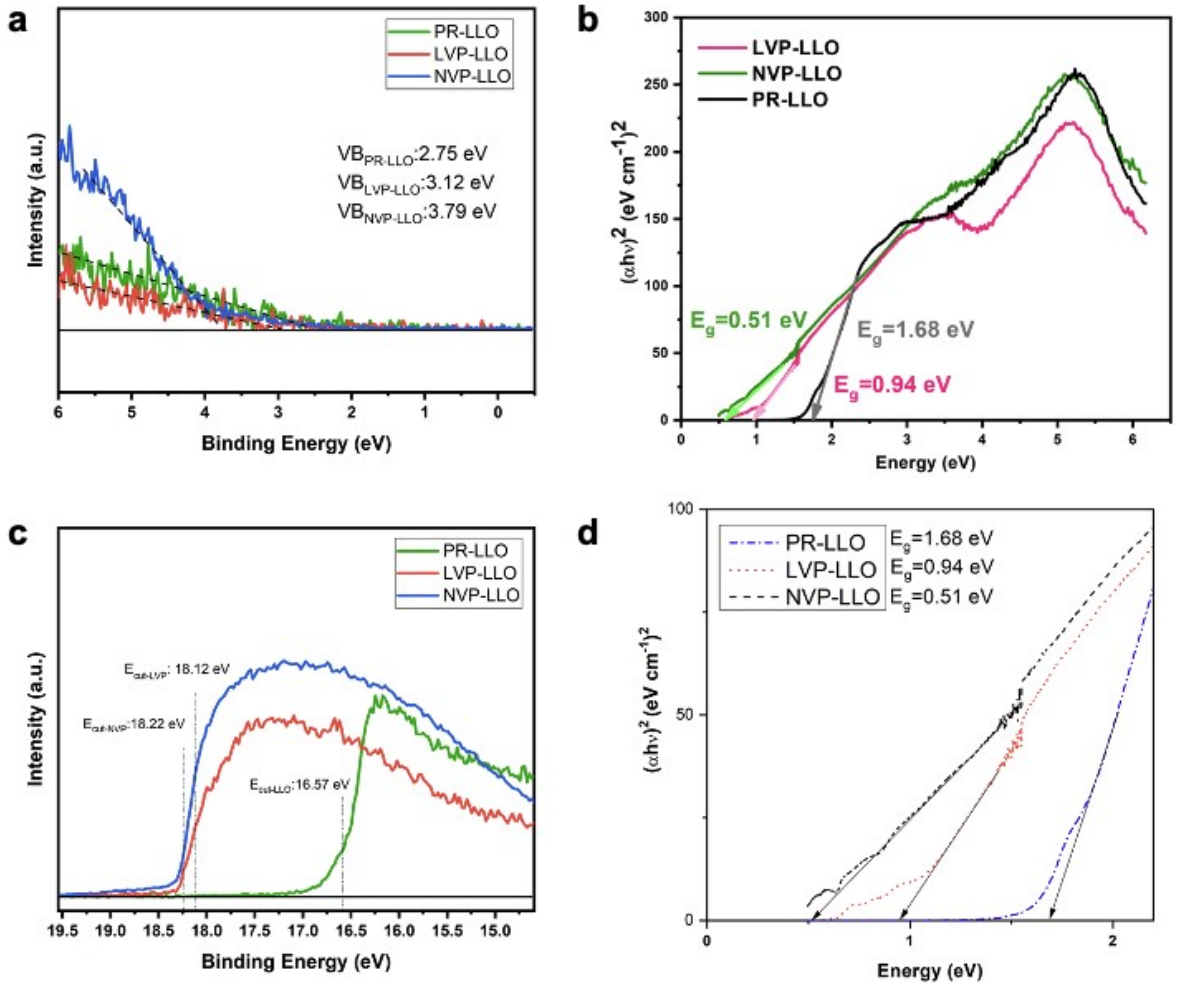

Figure S6. expanded views of the a) UPS He I secondary electron cutoff energy measured using ½ maxima of cut-off peak intensity, and c) UPS He I valence band maximum energy measured by the intersection of the final vertical linear region with the zero-intensity line for PR-LLO, LVP-LLO and NVP-LLO. In addition the Tauc plot b) Expanded and c) zoomed view of the are presented

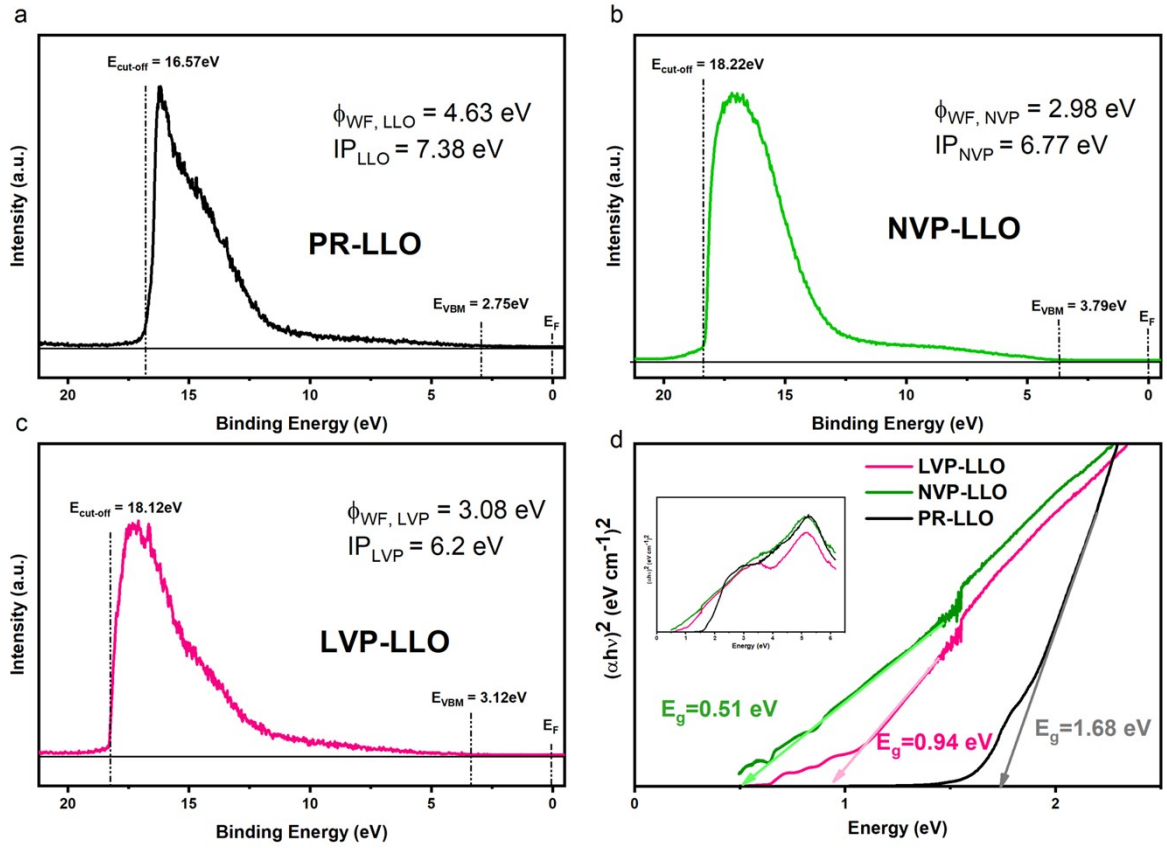

Figure S7. He I UPS spectra of a) PR-LLO, b) LVP-LLO and c) NVP-LLO with measured Ionization Potential (IP) and Work Function (WF) shown. d) Tauc plots for PR-LLO (black), LVP-LLO (pink) and NVP-LLO (green) samples with primary bandgap transitions and secondary optical transitions highlighted

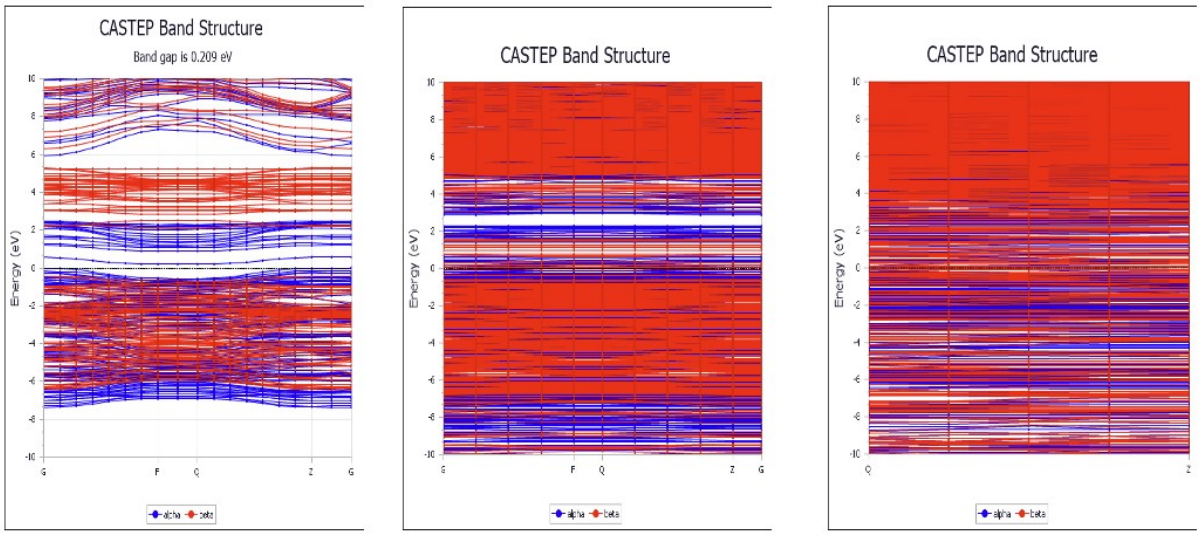

Figure S8. DFT-generated spin-polarized band structures of PR-LLO, LVP-LLO and NVP-LLO calculated using the sX-LDA Functional with majority spin bands shown in blue and minority spin bands shown in red.

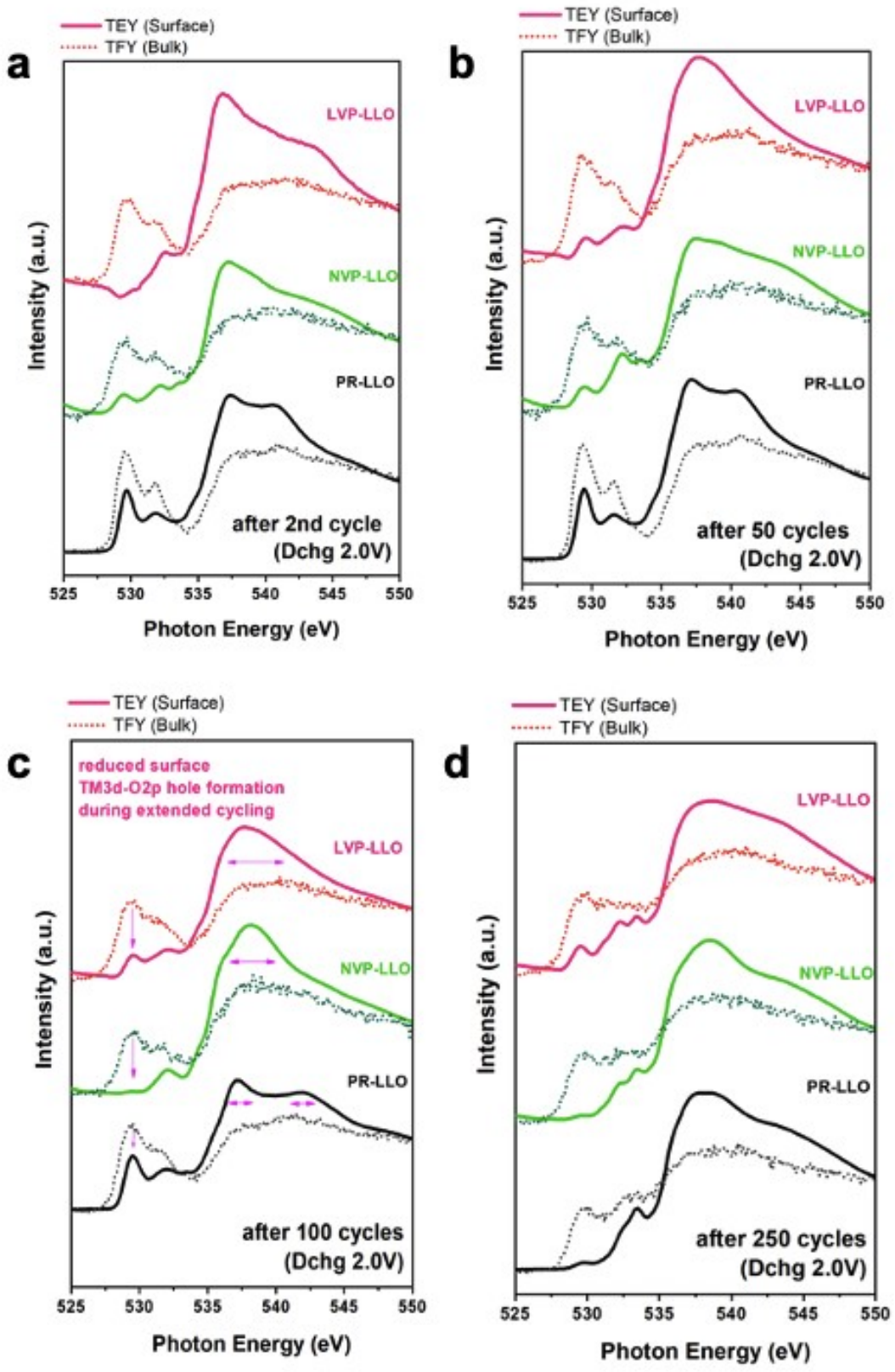

Figure S9. O K-edge XAS spectra collected in TEY and TFY modes at extended cycling for PR-LLO, LVP-LLO and NVP-LLO samples

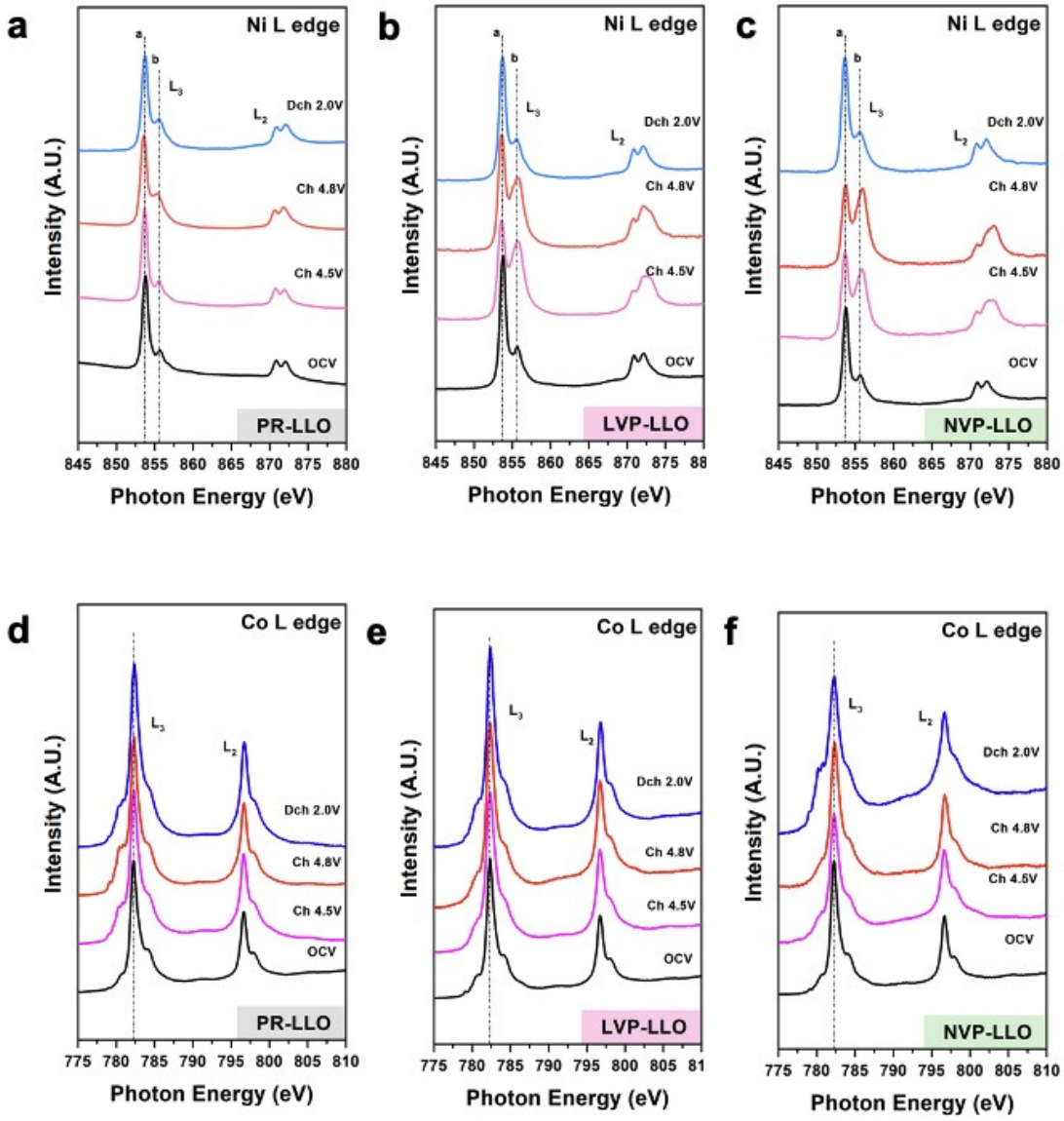

Figure S10. Ni and Co L-edge XAS spectra collected in TEY modes during initial charge-discharge for PR-LLO, LVP-LLO and NVP-LLO samples

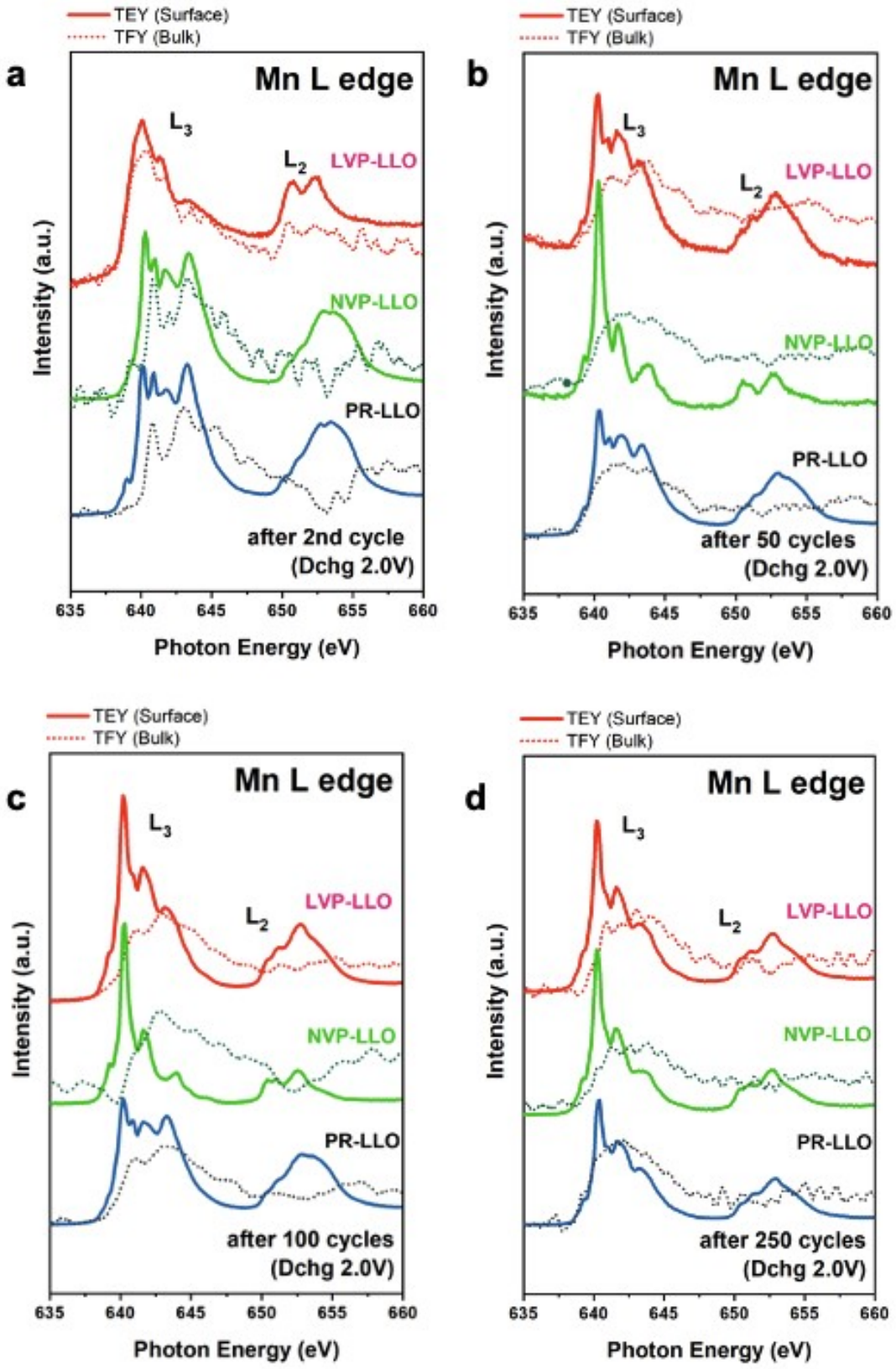

Figure S11. Mn L-edge XAS spectra collected in TEY and TFY modes at extended cycling for PR-LLO, LVP-LLO and NVP-LLO samples

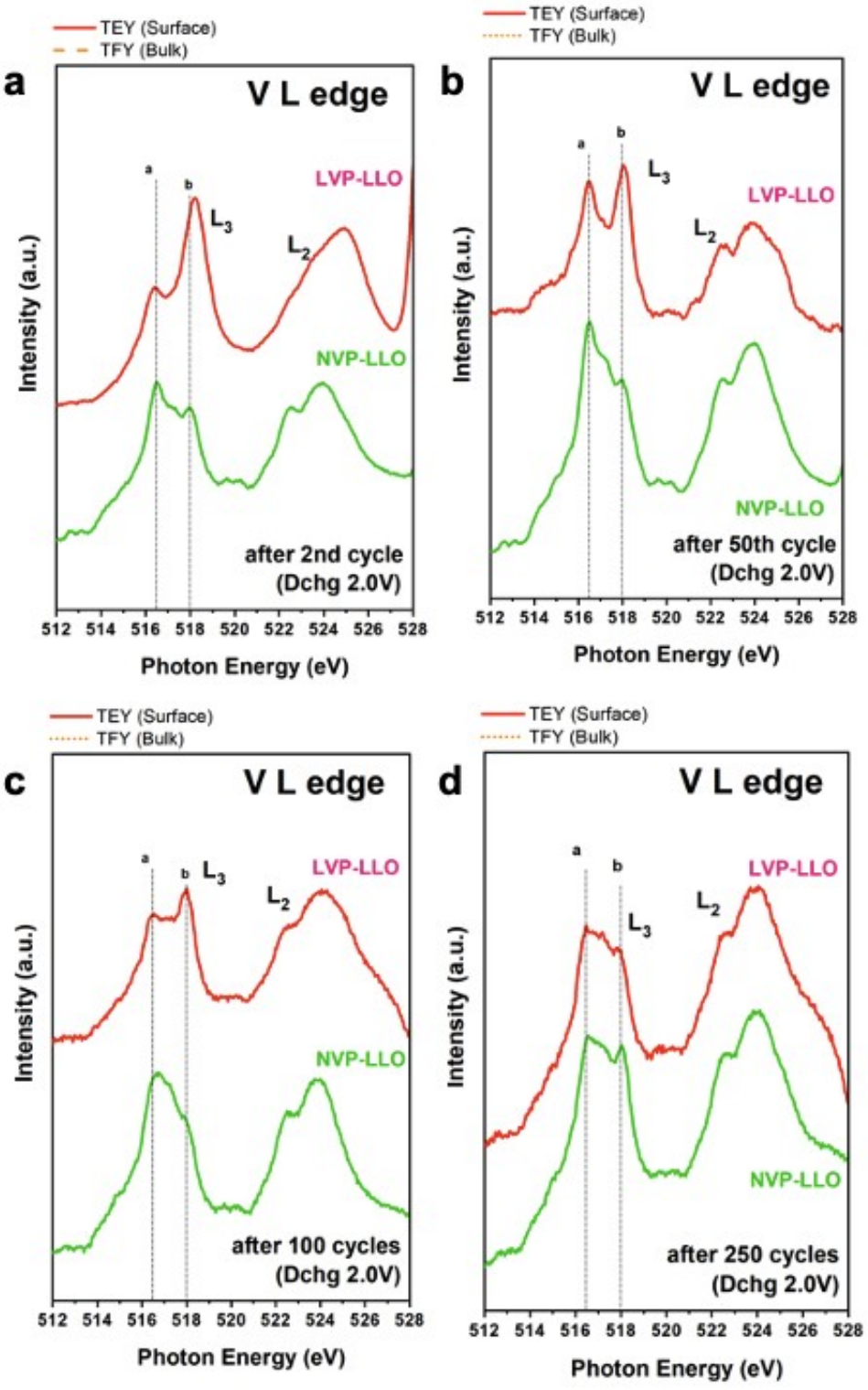
a
V L edge
TEY (Surface)
TFY (Bulk)
LVP-LLO
NVP-LLO
L3
L2
a
b
Intensity (a.u.)
after 2nd cycle
(Dchg 2.0V)
512 514 516 518 520 522 524 526 528
Photon Energy (eV)
b
V L edge
TEY (Surface)
TFY (Bulk)
LVP-LLO
NVP-LLO
L3
L2
a
b
Intensity (a.u.)
after 50th cycle
(Dchg 2.0V)
512 514 516 518 520 522 524 526 528
Photon Energy (eV)
c
V L edge
TEY (Surface)
TFY (Bulk)
LVP-LLO
NVP-LLO
L3
L2
a
b
Intensity (a.u.)
after 100 cycles
(Dchg 2.0V)
512 514 516 518 520 522 524 526 528
Photon Energy (eV)
d
V L edge
TEY (Surface)
TFY (Bulk)
LVP-LLO
NVP-LLO
L3
L2
a
b
Intensity (a.u.)
after 250 cycles
(Dchg 2.0V)
512 514 516 518 520 522 524 526 528
Photon Energy (eV)

Figure S12. V L-edge XAS spectra collected in TEY and TFY modes at extended cycling for PR-LLO, LVP-LLO and NVP-LLO samples

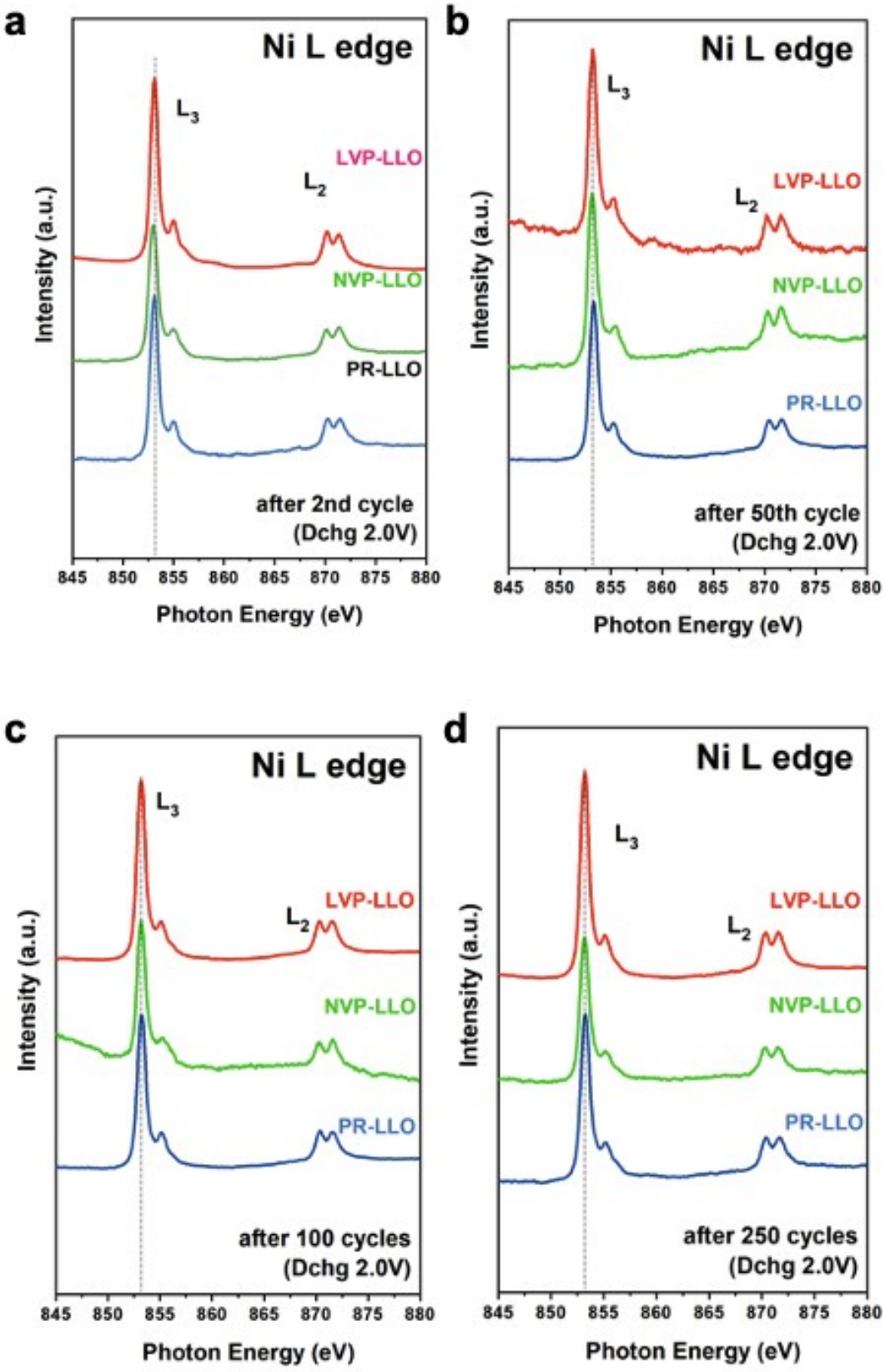

Figure S13. Ni L-edge XAS spectra collected in TEY mode at extended cycling for PR-LLO, LVP-LLO and NVP-LLO samples

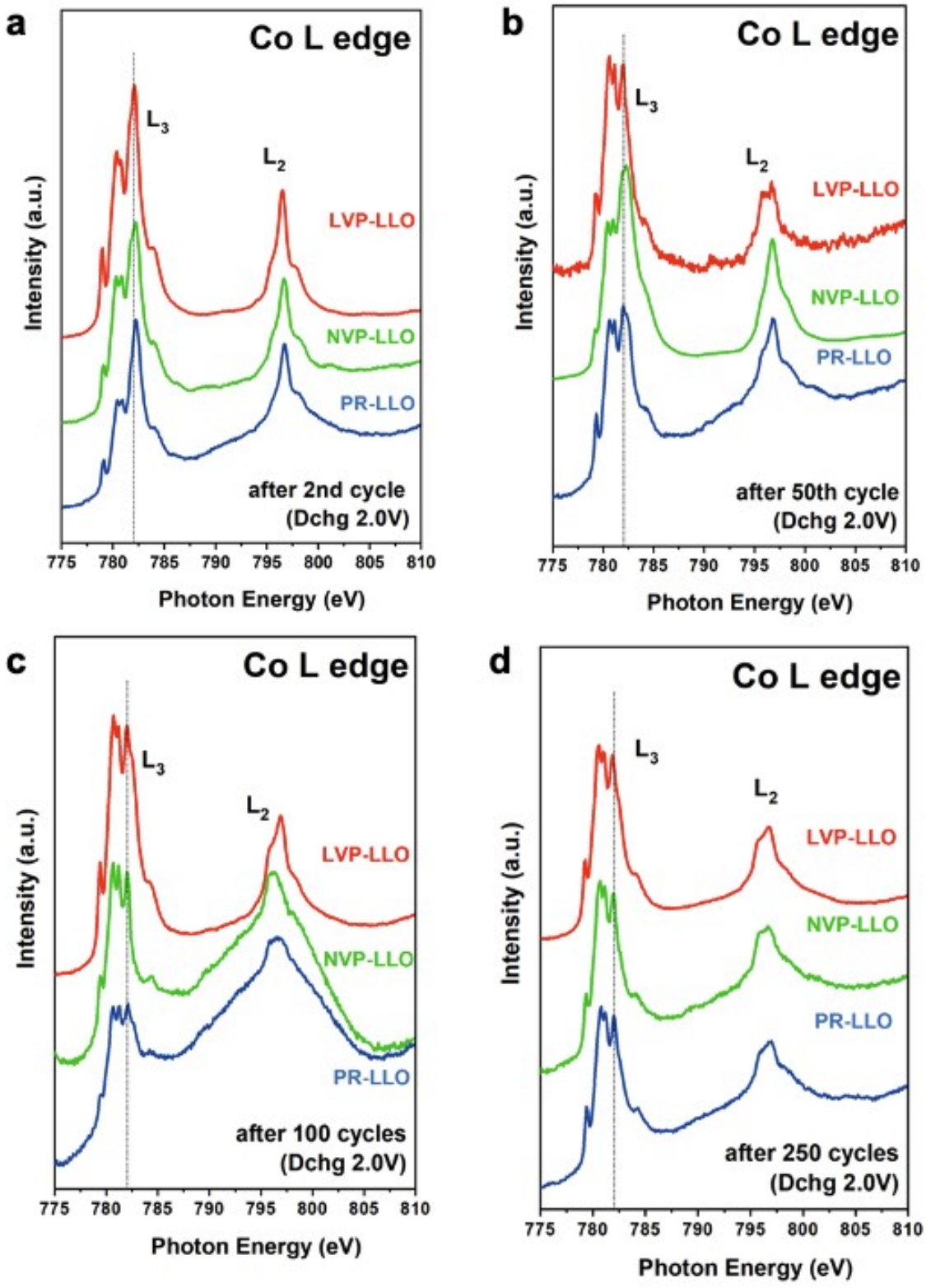

Figure S14. Co L-edge XAS spectra collected in TEY and TFY modes at extended cycling for PR-LLO, LVP-LLO and NVP-LLO samples

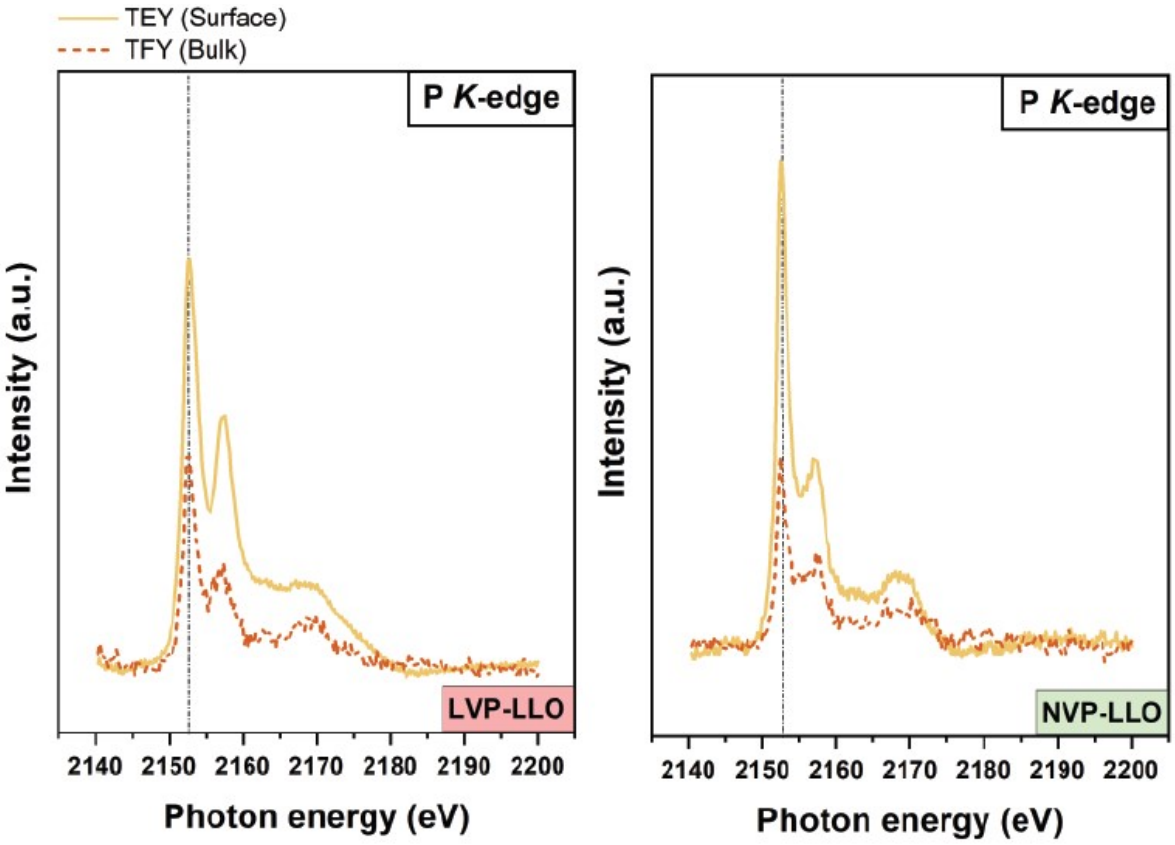

Figure S15. P K-edge XAS spectra collected in TEY and TFY modes for as-synthesized LVP-LLO and NVP-LLO coated samples

Supporting Tables:

Table S1 – Summary of ICP-OES for PR-LLO, LVP-LLO and NVP-LLO as-prepared powder samples

Element	**PR-LLO**	**LVP-LLO**	**NVP-LLO**
Symbol	Atomic %	Atomic %	Atomic %
Mn	71.19	62.92	64.99
Ni	15.25	16.51	16.66

Co	13.56	14.12	13.34
V	--	3.75	2.06
P	--	2.70	1.60
Na	--	-	1.35

Table S2 – Rietveld refinement results for XRD patterns collected from PR-LLO, LVP-LLO and NVP-LLO samples with refined unit cell parameters corresponding the $R\bar{3}M$ $LiTMO_2$ space group.

Sample	**PR-LLO**	**LVP-LLO**	**NVP-LLO**
a/Å	2.8512195	2.8534267	2.8569013
b/Å	0.0000000	0.0000000	0.0000000
c/Å	14.2360508	14.2104670	14.1906066
Density (g/cm3)	255.858	255.858	255.858
Volume (Å^3)	100.22625	100.20108	100.30488
Rp	1.67	1.32	1.58
Rwp	1.85	1.80	2.33
Rexp	0.77	0.77	0.79
G.O.F.	2.48	2.33	2.80
I(003)/I(104)	1.48	1.33	1.23

Table S3 - Electrochemical Impedance spectroscopy circuit model data for PR-LLO, LVP-LLO and NVP-LLO samples

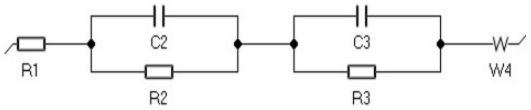

Sample	PR-LLO	LVP-LLO	NVP-LLO
Re/Ω	4.22	5.28	5.62
Rs/Ω	57.35	35.83	58.94
Rct/Ω	39.19	21.684	19.236
W	80.08	49.399	50.88

References:

1. Maheu, C.; Cardenas, L.; Puzenat, E.; Afanasiev, P.; Geantet, C., Ups and Uv Spectroscopies Combined to Position the Energy Levels of Tio2 Anatase and Rutile Nanopowders. *Physical Chemistry Chemical Physics* **2018**, *20*, 25629-25637.
2. Schreiber, M.; Toyozawa, Y., Numerical Experiments on the Absorption Lineshape of the Exciton under Lattice Vibrations. Iii. The Urbach Rule. *Journal of the Physical Society of Japan* **1982**, *51*, 1544-1550.
3. Bhola, K.; Varghese, J. J.; Dapeng, L.; Liu, Y.; Mushrif, S. H., Influence of Hubbard U Parameter in Simulating Adsorption and Reactivity on Cuo: Combined Theoretical and Experimental Study. *The Journal of Physical Chemistry C* **2017**, *121*, 21343-21353.